1 **Determining the depth and upwelling speed of the equatorial Ekman layer from**
2 **surface drifter trajectories**

4 Nathan Paldor[1] and Yair De-Leon[1]

6 [1]Fredy and Nadine Herrmann Institute of Earth Sciences
7 Hebrew University of Jerusalem
8 Edmond J. Safra Campus, Givat Ram, Jerusalem, 9190401 Israel

13 Correspondence to: N. Paldor (nathan.paldor@mail.huji.ac.il)

18 **Abstract**

19 Trajectories of 500 - 600 drogued surface drifters launched since 1979 in the equatorial ocean are
20 analyzed by employing the results of a new Lagrangian theory of the poleward transport from the
21 equator forced by the prevailing Trade winds. The Lagrangian theory provides an explicit expression for
22 the depth of the Ekman layer that circumvents the application of the 3-Dimensional continuity equation
23 that requires calculating the divergence of horizontal transport, which was the basis of all previous
24 studies on the subject. The analysis is carried out for drifters launched within 1° of the equator that
25 reached final latitude of 3°, 4° or 5° North or South of the equator while remaining in one hemisphere
26 throughout the entire travel time. The analysis yields robust estimates of 45 meters for the Ekman layer's
27 depth and 1.0 meters per day for the upwelling speed of deep water into the layer.

1. Introduction

The Trade winds that blow westward in the Tropics as part of the Hadley circulation are the first and basic component of the heat transport from the warm equatorial surface ocean to the cold poles that mitigates the overall pole-to-equator temperature gradient on Earth. The mechanism that enables the poleward time-independent heat transport is the surface flow in the ocean that is directed 90° to the right/left of the wind in the northern/southern hemisphere relative to the direction of the overlying wind. This counter-intuitive flow direction results from Earth's rotation that adds the Coriolis force to the stress applied by the winds at the ocean surface. This straightforward scenario of wind-driven ocean circulation appears in all textbooks (Knauss, 1996; Talley et al., 2011) but despite its convincing simplicity, currently, quantitative estimates of the parameters that control it vary widely depending on the data and method used in the calculations of these estimates.

The classical theory that describes the ocean response to forcing by the overlying winds was developed about 120 years ago by V.W. Ekman under the assumption of constant Coriolis frequency (Ekman, 1905). This assumption greatly simplifies the analysis by ensuring that all coefficients in the governing equations are constant. The dynamics described in Ekman's theory includes a steady flow perpendicular to the wind direction and inertial, i.e. force-free, oscillations at the local (constant) Coriolis frequency. This is in sharp contrast to the equatorial region where the Coriolis frequency vanishes at the equator and varies (linearly) with latitude, which turns the equations nonlinear so the oscillation-free flow is not steady as in Ekman's original mid-latitude theory. The poleward directed surface flows in both hemispheres along the equator imply a strong horizontal divergence along the equator which can only be balanced by the upwelling of deeper water into the wind-forced, Ekman, layer. Though the heuristic application of the mid-latitude Ekman theory to the vicinity of the equator is quite straightforward, to-

51   date, it could not be employed to estimate either the depth of the equatorial Ekman layer or the rate of

52   upwelled volume of water.

53   The complications that result from the inclusion of the meridional variation of the Coriolis frequency in

54   Ekman's theory were recently resolved in a theory of wind-driven flow in which Ekman's 1905 classical

55   theory was extended to the equatorial region (Paldor, 2024). This new theory employs the adiabaticity

56   method (Goldstein, 1980; Paldor and Friedland, 2023) that filters out fast oscillatory dynamics from the

57   slow dynamics associated with the motion of the center of oscillation. The application of this general

58   method to the equatorial Ekman problem filters out the oscillation that result from the meridionally

59   varying Coriolis force from the slow and monotonic poleward motion of a water column forced by the

60   combination of the wind stress and the Coriolis force. The essence of the method is the formulation of

61   the problem as the dynamics of a (quasi-)particle about the minimum of a potential while the potential

62   itself varies with time on a slower time scale than the period of oscillations about the minimum. The

63   potential is derived from the meridional Lagrangian momentum equation when the zonal velocity, $\underline{U}$, is

64   expressed as $U = D + \int f(y)dy$ where $f(y)$ is the latitude-dependent Coriolis frequency ($= \beta y$) and D is

65   the pseudo angular momentum, which is conserved in the absence of other (body) forces. The

66   substitution of the angular momentum for the zonal velocity is essential for the analysis in spherical

67   coordinates RomKedar et al. (1997). Additional details of the theory are given in Sect. 2.1.

68   Direct observations of the depth (thickness) of the equatorial Ekman layer and the rate of upwelling

69   water to it are hard to quantify due to the poor observational definition of the layer's dimensions and the

70   extremely low speed of upwelling. Halpern and Freitag (1987) estimated the upwelling rate in the eastern

71   equatorial Pacific Ocean above 50 m depth to be about 2 m day^{-1} from the divergence of several moored

72   horizontal current meters. Below 50 m depth their estimated vertical velocity is negative (directed

73   downward). A similar upwelling rate of 2 m day^{-1} extending to depths of 120 m was estimated by Halpern

74   et al. (1989) between 110°W and 140°W from 12/1983 to 9/1984 (but excluding 4/1984) using the same

75   method of inferring vertical speeds from the divergence of horizontal currents measured by moored

76   current meters. The upwelling speed decreased eastward in these observations and the variation of the

77   observed values greatly exceeded the mean values. In the same region (Central Pacific) but in 2-3/1980

78   Bubnov (1989) used a similar observation method of integrating the 3D continuity equation associated

79   with observed horizontal currents, and estimated the upwelling velocity over the upper 300 m to vary

80   between 1 and 8 m day^{-1}.

81   Surface drifter trajectories deployed in the Eastern Pacific during 1977-1982 were used by Hansen and

82   Paul (1987) as proxies of the currents and the trajectory divergence as a proxy of the current's

83   divergence, which resulted in an estimate of 1.5 m day^{-1} for the upwelling velocity in a stripe of $\pm 1.5°$ of

84   the equator. For their interpretation they assumed that the drifter trajectories represent the currents and

85   divergence in the top 50 m. As noted by the authors, the main issue with their analysis is the accuracy of

86   representation of currents by drifter trajectories. Using over 700 drifters launched between 1979 and

87   1990 Poulain (1993) estimated an upwelling velocity of $15 - 20$ m day^{-1} between 90°W and 150°W in

88   the equatorial Pacific. The method used by Poulain (1993) in the interpretation of drifter observations is

89   to average the drifter velocities in given geographical domains and at selected time intervals to generate

90   the Eulerian velocities at the center of the domain at that time. The high values of upwelling velocity in

91   this study result from the small areas used for inverting the observed Lagrangian drifter velocities to

92   Eulerian fields. Two important conclusions emerge from that study: The first is that except for its western

93   part, the horizontal divergence in the equatorial Pacific is quite uniform and therefore so should be the

94   upwelling speed. The second is that the upwelling velocity decreases monotonically with the assumed

95   width of the meridional band over which the horizontal divergence is calculated.

96   Estimates of upwelling rates were also calculated based on the distribution of ^{14}C released in large

97   amounts to the atmosphere between 1955 and 1963 when above-ground nuclear tests took place. An

98   analysis of the oceanic uptake of ^{14}C and its redistribution in the Pacific Ocean carried out by Quay et al.

99   (1983) yielded an estimate of about 0.3 m day^{-1} for the upwelling velocity along the equator. Aside from

100   this geo-isotopic study the previous estimations of the horizontal divergence fields were estimated either

101   directly from current meter observations or indirectly from drifter trajectories. In the latter case that data

102   were either spatially averaged to yield the Eulerian fields or interpreted as proxies of these fields. In

103   contrast, the current study applies a recently developed Lagrangian dynamical theory directly to observed

104   drifter trajectories which bypasses the need to estimate first the horizontal divergence. The large number

105   of drifters, the accurate tracking of their location by satellites and the longtime of coverage allows for a

106   selection of sufficient number of drifter trajectories that satisfy pre-determined selection criteria and

107   yields accurate estimates of the depth of the equatorial Ekman layer and the speed of upwelling into it.

108   The application of the Lagrangian theory to drifter observations and the data used in this study are

109   detailed in Section 2. In Section 3 we give the results obtained by applying the theory to drifter

110   trajectories and the study is summarized in Section 4.

111   **2. Theory and Data**

112   **2.1. Theory**

113   The recent extension of the wind-driven theory of ocean circulation to the equator described in Paldor

114   (2024) has demonstrated that, as in Ekman's original theory, the oceanic response can be decomposed

115   into a monotonic, slow, flow (which is directed poleward in the equatorial region) and fast, large

116   amplitude, oscillations. In contrast to Ekman's original theory, in the equatorial region when the wind

117   stress is directed westward the oscillations are highly nonlinear and of large amplitude. An example of the

118   large amplitude inertial oscillations associated with an initial westward directed velocity when no wind

119   stress affects the motion is shown in Fig. 1a. The present study applies the explicit expressions developed

120   in Paldor (2024) to the observed trajectories of surface drifters and employs the nondimensional

121   variables and parameters in Eq. 10 of Paldor (2024). The dimensional counterpart of this equation is:

122
$$\frac{dy}{dt} = \frac{1}{y(t)} \frac{-\tau^x}{H} \left(\frac{R_e}{2\Omega\rho}\right).$$
(1)

123   Here, y(t) is the distance from the equator at time t. The global parameters in this relation are: $\rho =$

124   1027 kg m^{-3} (water density) $\Omega = 7.29 \cdot 10^{-5}$ s^{-1} and $R_e = 6371 \cdot 10^3$ m (Earth's rotation frequency

125   and radius, respectively) so $\left(\frac{R_e}{2\Omega\rho}\right) = 4.25 \cdot 10^7$ m^4 s kg^{-1}. The remaining, particular, parameters are: τ^x

126   - the wind stress (units: N m^{-2}; negative for easterly winds) and H (m) - the Ekman layer's depth.

127   Multiplying the nonlinear relation (1) by $y(t)$ and integrating the resulting 1st order equation for $y(t)^2$

128   yields:

129
$$y(t)^2 = y(0)^2 + 2\frac{-\tau^x}{H} \cdot \left(\frac{R_e}{2\Omega\rho}\right) t.$$
(2)

130   As demonstrated in Fig. 1b, this expression (shown by the red curve) successfully filters out the inertial

131   oscillations from the actual latitude time-series (blue curve), and describes the net, oscillation-free, i.e.

132   the poleward motion when the inertial oscillations shown Fig. 1a are filtered out.

133   Setting t in Eq. (2) to t_i, the travel time of drifter #i, $y(t)$ to L, a "boundary" of the equatorial region,

134   and inverting the equation to an explicit expression for H yields the estimate of H based on trajectory #i:

135
$$H = \left(\frac{R_e}{2\Omega\rho}\right) \frac{2(-\tau^x)}{L^2 - y_i(0)^2} t_i,$$
(3)

136   where $y_i(0)$ is the distance of drifter #i from the equator at $t = 0$ (i.e. the distance of the launch point

137   from the equator). The values of H are calculated from this equation for each drifter and then averaged

138   to yield the mean value for the particular value of L.

139   **2.2. Drifter trajectories**

140   Nearly 30,000 surface drifters were released from 1979 at the ocean surface (Lumpkin et al., 2017) and

141   the geographical trajectories of these drifters are tracked by satellites every 6 hours for periods of up to

142 1000 days. These (Lagrangian) observations cover the global ocean and a few percent of them were

143 launched on both sides of the equator in the Pacific, Atlantic and Indian oceans. The slightly negatively

144 buoyant drifter is typically drogued at 15-meter depth, so it provides an estimate of the current in the top

145 15 meters of the water column where the wind stress is the primary forcing (Lumpkin et al., 2017). The

146 agreement between drifter trajectories and ocean currents demonstrated in Lagerloef et al., (1999) and

147 assumed in Poulain (1993) motivates an analysis of observed drifter trajectories in order to determine the

148 depth of the equatorial Ekman layer and the upwelling speed of deep water into it.

149   The drifter trajectories used in the analysis are freely available from NOAA Global Drifter Program

150 (NOAA/AOML/GDP) site. The data were screened according to the following three criteria:

151   1. They were launched within $1° \approx 110$ km south or north of the equator (regarded as the equator).

152   2. The drifters remained in one hemisphere throughout the entire travel time to the final latitude

153   (equator crossing is not allowed under westward directed wind stress).

154   3. The drifters were continuously tracked, with gaps no longer than one day, during their motion from

155   the launch point to the final latitude that marks the boundary of the equatorial region (i.e. $3° \approx$

156   330 km, $4° \approx 440$ km or $5° \approx 550$ km).

157 The latitudes $3°$ and $4°$ were used in previous studies to define the boundaries of the equatorial region

158 (Brady and Bryden, 1987; Lagerloef et al., 1999; Johnson et al., 2001) but in the present study we also

159 used $L = 5° \approx 550$ km to verify the robustness of the calculated averages to the selected values of L.

160 The case $L = 2°$ is not included in the analysis since the singularity of Eq. (3) at $L^2 = y_i(0)^2$ affects the

161 accuracy of the estimates of H when L is close to $y_i(0)$ i.e. for $L = 2° \approx 220$ km (and for $y_i(0) \leq 1°$) the

162 denominator is tiny which can yield extremely high value of H and amplify observational errors.

163   Of the ~30,000 drifter trajectories archived in AOML archive as of 8/2024, over 1500 drifters were

164 launched near the equator and reached the final latitude ($3°, 4°$ or $5°$) out of which ~700 drifters

165 remained in one hemisphere. The number of drifters in the Atlantic and Pacific oceans that reached each

166   of the final latitudes is given in the 2nd column of Table 1 that also gives the mean $y_i(0)$ (3rd column) and

167   the mean t_i, (4th column) to the final latitudes (noted in the rows of this table). The Indian Ocean is

168   excluded from the analysis due to the positive mean annual wind stress in it (see Sect. 2.3). No

169   information is available on the fraction of drifters that lost their drogues on their way from $y_i(0)$ to L.

170   **2.3. Wind stress**

171   The daily wind stress values over the oceans, τ^x, used in this work are available at NOAA/CoastWatch site

172   in 0.125° spatial resolution for the period 1999-2009. We calculated the averaged wind stress in the

173   region of the Indian, Atlantic and Pacific oceans in a zonal strip that straddles the equator between $-L$

174   and $+L$, where L corresponds to 3°, 4° or 5°.

L (degrees)	Number of drifters	Mean $y_i(0)$ (degrees)	Mean t_i (days)	τ^x (Nm^{-2})	Mean H (m)	$W = \frac{H}{t_i} \cdot \frac{L - y_i(0)}{L}$ (m day^{-1})
3.04	610	0.29	29.67	-0.0261	51.10	1.56
4.04	576	0.29	43.43	-0.0264	42.48	0.91
5.04	531	0.29	58.12	-0.027	37.16	0.60

175

176   **Table 1: Drifter characteristics in the Pacific and Atlantic oceans and the zonal wind stresses there. The**
177   **shown values of L are larger by a few kilometers compared to the distances corresponding to 3°, 4° or**
178   **5° since a drifter is determined to be "at L" with an offset of up to 6 hours after its passage of that**
179   **point. Less than 10% percent of the relevant drifters were launched in the Indian ocean which is not**
180   **included in this table and in the analysis since the annual mean wind stress in the Indian Ocean is**
181   **directed eastward, which is inconsistent with a poleward directed net motion.**

182   These averages are given in the 5th column of Table 1 for the Atlantic and Pacific oceans, where the values

183   are nearly identical (they differ by no more than a few percentage points) but not for the Indian ocean

184   where the calculated mean values are positive (so $H < 0$) and small (less than $+0.01$ N m^{-2}) probably

185   due to the strong seasonal forcing by the Monsoon system that induces eastward directed zonal winds

186   throughout part of the year in this ocean (Hastenrath and Polzin, 2004; Zhang et al., 2022). The decade-

187   long zonal wind stress observations are considered representative of the climatic values that prevailed

188   throughout the trajectories of all drifters. Though the mean negative values of τ^x in the Atlantic and

189   Pacific Oceans are not uniform (reaching their maximal values in the center of each ocean and tapering

190   off near the continents that bound the ocean on the east and west sides) only the mean values are used.

3. Results

192   Four representative drifter trajectories are shown in Fig. 2 and they demonstrate the richness of observed

193   trajectories near the equator, the intricate combination of oscillations with slow poleward propagation

194   and the occurrence of equatorial crossing in many trajectories.

195   Substituting the values of $y_i(0)$ and t_i for each drifter in Eq. (3) and averaging these values over all

196   relevant drifters yields the values of H given in the 6$^{\text{th}}$ column of Table 1. The histograms of the H values

197   for each value of L are shown in Fig. 3 so the value of H is best estimates by: $H = 44 \pm 7 \approx 45$ m.

198   Equation (2) can also be employed to calculate the poleward, oscillation-free, velocity of a drifter on

199   its way from $y_i(0)$ to $L = y(t_i)$ from the drifter's average speed during its travel: $V = \frac{L - y_i(0)}{t_i}$. Thus, the

200   volume divergence (per unit length in x) that results from the anti-parallel, poleward directed, volume

201   fluxes of 2 water columns that are initially conjoined along the equator and move poleward is $2HV =$

202    $2H\frac{L - y_i(0)}{t_i}$. The vertical volume flux (per unit length) due to Ekman upwelling during t_i is: $2LW$, where W

203   is the upwelling speed. Equating the vertical and horizontal fluxes yields $WL = H\frac{L - y_i(0)}{t_i}$ or $W = \frac{H}{t_i}\frac{L - y_i(0)}{L}$.

204   The mean values of H and t_i in Table 1 then yield the mean value of $W \approx 1.0$ m day^{-1} for the three

205   values of L.

206   The estimated H and W values along the equatorial Atlantic and Pacific Oceans are noted in Fig. 4 on a

207   qualitative, textbook, cartoon of the wind forcing and resulting oceanic flow patterns.

4. Summary and Discussion

209   The mean estimates of $H = 45\ m$ and $W = 1\ m\ day^{-1}$ calculated here based on surface drifter

210   trajectories are more robust compared to prior estimates derived from standard hydrographic

211   observations. Table 1 shows that the present estimates of H vary with L by a few meters and those for W

212   by about 0.5 $m\ day^{-1}$. These variations are smaller than those of estimates based on standard

213   hydrographic data that can vary by about one order of magnitude (Wyrtki, 1981; Brady and Bryden, 1987;

214   Lukas and Lindstrom, 1991; Weingartner and Weisberg, 1991). As an example, the $H = 45\ m$ value

215   reported here exceeds the estimate of 30-40 m proposed in Lukas and Lindstrom (1991) but the O(10%)

216   variation of the present estimate is significantly smaller than the O(80%) variation in the previous

217   estimate. In view of the crucial role played by the poleward flow of warm equatorial water in mitigating

218   the large radiative pole-to-equator temperature gradient (Czaja and Marshal, 2006; Hartmann, 2016) a

219   reliable quantification of the initiation of this flow is important for understanding Earth's climate.

220   The zonal stress is not uniform, reaching a maximal value in the center of the Ocean and tapering off

221   towards the boundaries on the east and west. The effect of this variation on the value of H Is pronounced

222   in the equatorial Pacific Ocean and calculations of H using the values of τ^x at each drifter's initial location,

223   yield a wider range of H values. These estimates, too, are not exact since the value of τ^x varies along the

224   drifter trajectory. A detailed analysis of the variation of τ^x along a drifter trajectory and its effect on the

225   value of H calculated in that trajectory are left for future work.

226   In contrast to Ekman's theory in mid-latitude, the extension of this theory to the equatorial region

227   implies that the slow net poleward motion of a water column subject to a zonal wind stress is

228   accompanied by a zonal component. This results naturally from the inertial oscillations that involve net

229   zonal translation on the equator (as in Fig. 1a), whereas in mid-latitudes inertial oscillations are not

230   accompanied by a translatory motion.

231   The results calculated in Sect. 3 focus on the net poleward propagation rate, which neglects the

232   inertial oscillations, while the observed trajectories include both types of motion. The neglect of inertial

233   oscillations in the observed trajectories is justified based on the fact that the period of these oscillations is

234   much shorter than the temporal length of the averaged trajectory used for calculating H in Eq. (3). The

235   high variability of the geographical trajectories, which is exemplified in Fig. 2, does not permit an estimate

236   of the oscillations' period directly from the trajectories. However, for the values of $\tau = 0.026\ Nm^{-2}$ and

237    $H = 45\ m$ the period of inertial oscillations can be estimated from the scale $T = \left(\beta \cdot \frac{\tau}{\rho H}\right)^{-\frac{1}{3}} \approx 5\ days$

238   which is much shorter than the typical 30-60 days trajectory length (see the values of t_i in Table 1). Thus,

239   during the relatively long drifter travel time the poleward motion due to the oscillations averages out to

240   zero, leaving the poleward motion of the oscillations' centers as the sole contributor to the net motion.

241   The results shown in Table 1 imply a decrease in the value H (and hence the value of W) with the increase

242   in L. This result is not trivial since Eq. (3) is also satisfied with constant H provided $L^2 \propto t_i$ for $y_i(0) \ll L$.

243   However, the calculated values of t_i for different values of L reported in Table 1 only show a power slightly

244   above 1.0 (but significantly smaller than 2.0). The variation of H with L probably originates from a

245   mechanism similar to that depicted in Fig. 4 where the depth of the Ekman layer becomes shallower with

246   the distance from the equator, which affects the $t_i(L)$ relation. Though no explanation is proposed here

247   for this dependence of H on L this result is consistent with the results reported in Fig. 3 of Poulain (1993),

248   which show that the horizontal divergence decreases monotonically with the width of the latitudinal band.

249   We also note that Eulerian calculations of $\frac{\partial v}{\partial y}$ based on spatial averaging of the Lagrangian observations as

250   was done in Poulain (1993) yield an estimate of W/H so additional information is needed for determining

251   each of these parameters (Poulain, 1993 arbitrarily assumed $H = 50\ m$). In contrast, in the present study

252   H is determined directly from drifter trajectories, which yields an estimate of W based on mass

253   conservation in a box of meridional extend L and depth (thickness) H (and unit zonal length).

254   The successful application of the new dynamical theory of wind-driven equatorial transport in the

255   ocean developed in Paldor (2024) lends credence to the relevance of this theory to observations in the

256   equatorial ocean. This relevance is demonstrated despite the negligence of important factors such as the

257   meridional wind stress (can be significant at short times), the initial drifter velocity (assumed to vanish in

258   the theory) or changes in the zonal wind stress. It can be argued that the calculation and successful

259   application of the oscillation-free speed of poleward wind-driven motion on the equator is of similar

260   significance to ocean dynamics as the development of the expression for the steady transport in the

261   original f-plane Ekman theory.

262

263   **Author contribution**:

264   NP: Initiation of project, writing various drafts and theoretical analysis.

265   YD: Data collection and analysis, editing and production of display items.

266   **Competing interests**: The authors declare that they have no conflict of interest.

267   **Financial support**: The authors happily declare that no funding was received for this study

268   **Data Availability**: The drifter data used in this study are maintained by NOAA/AOML and the

269   wind stress data are maintained by NOAA/CoastWatch, both sites are noted in the list of

270   references

271   **Acknowledgements:** The authors are grateful to two anonymous reviewers whose comments

272   greatly improved the presentation of this paper.
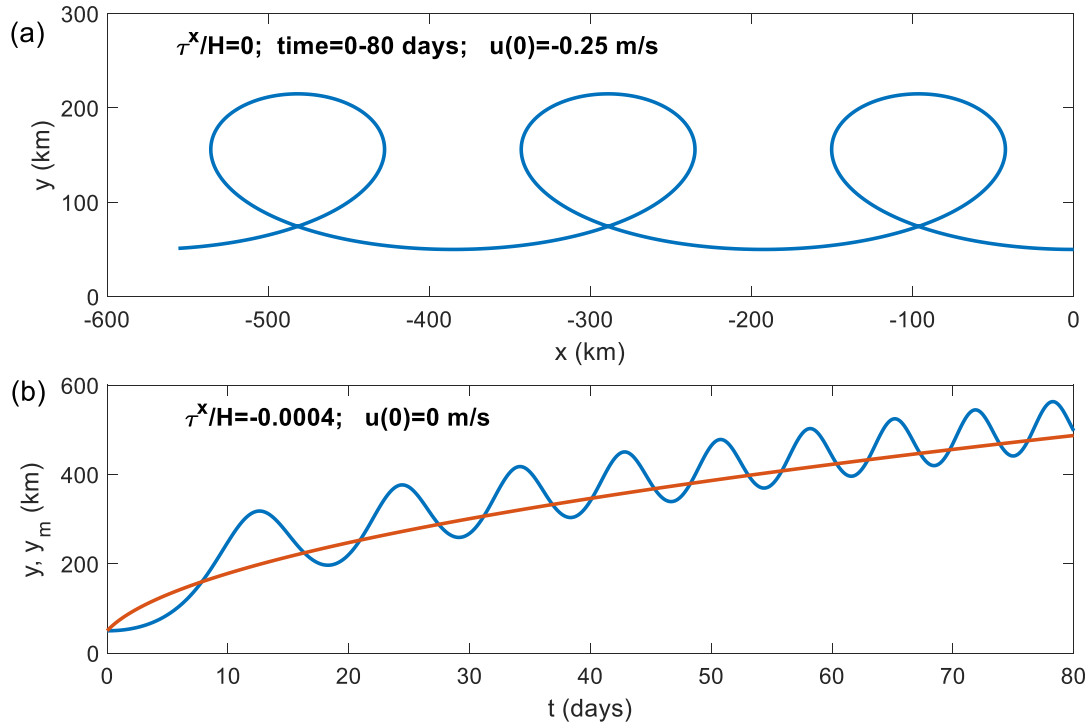
273
274 Figure 1: Panel (a): The numerically calculated geographic trajectory of a water column initiated
275 with a westward directed zonal velocity of 0.25 m s^{-1} subject only to the, latitude-dependent,
276 Coriolis force. Panel (b): the latitude (i.e. distance from the equator in km) time-series (blue curve)
277 and the oscillation free latitude time-series given by Eq. (2) denoted here by y_m (red curve) of a 50 m
278 deep water column forced by a westward directed wind stress, τ^x, of 0.02 N m^{-2}. In both panels the
279 initial distance from the equator is $y(0)=50$ km while the initial longitude and the initial meridional
280 velocity are both 0.
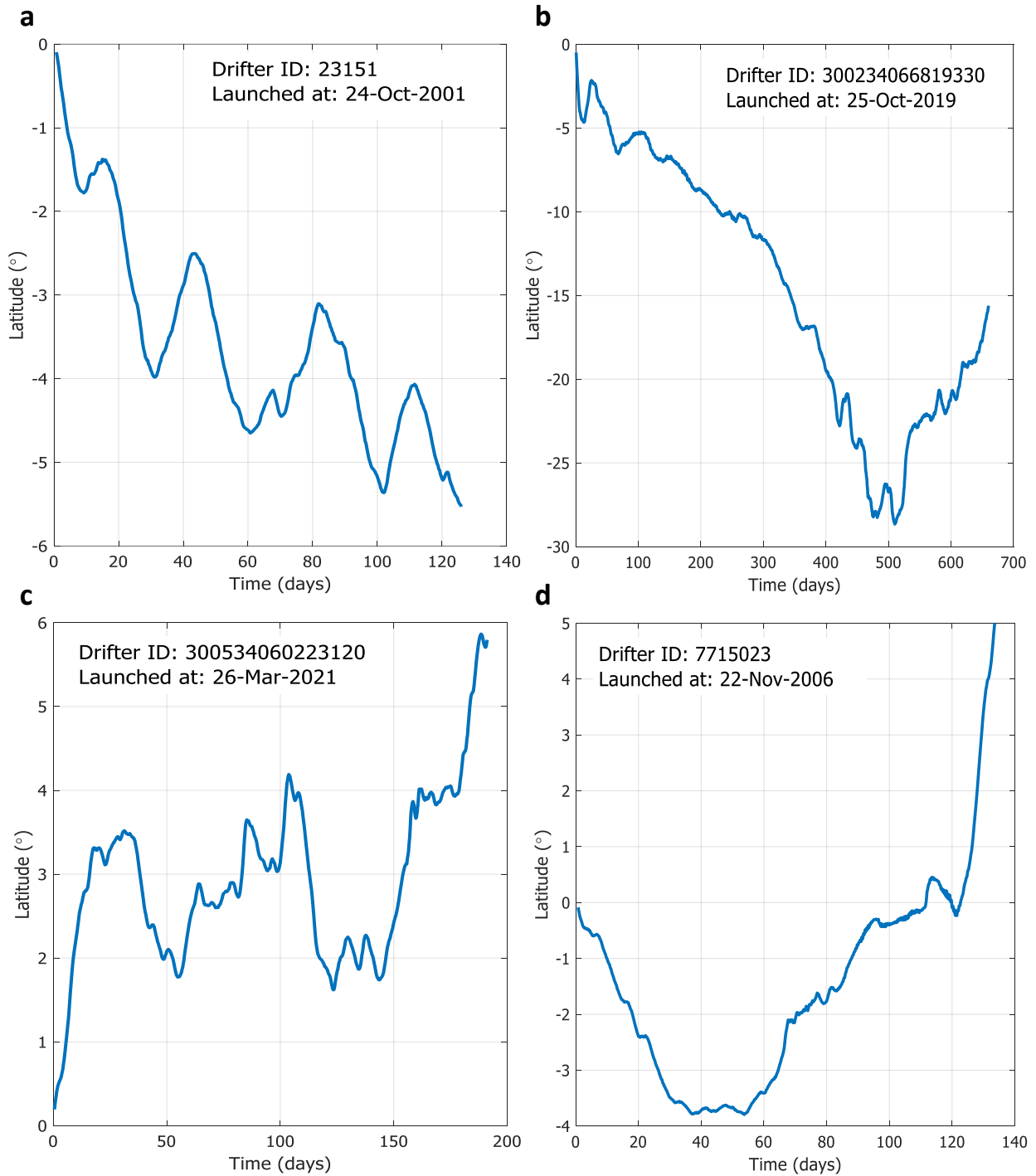
Figure 2: Four drifter trajectories originating within $1°$ of the equator analyzed in this study. a) A typical southern hemisphere trajectory that clearly shows oscillations and a mean poleward flow; b) A fast southern hemisphere trajectory that reaches $4°$ in just a few days and remains operational for nearly 2 years; c) A slow northern hemisphere trajectory that reaches $4°$ in more than 100 days; d) Part of a trajectory that reaches $3°$ prior to crossing the equator so it is included in the analysis of $L = 3°$ but not in the $L = 4°$ or $L = 5$ analyses since it reaches these latitudes only after crossing the equator.

287
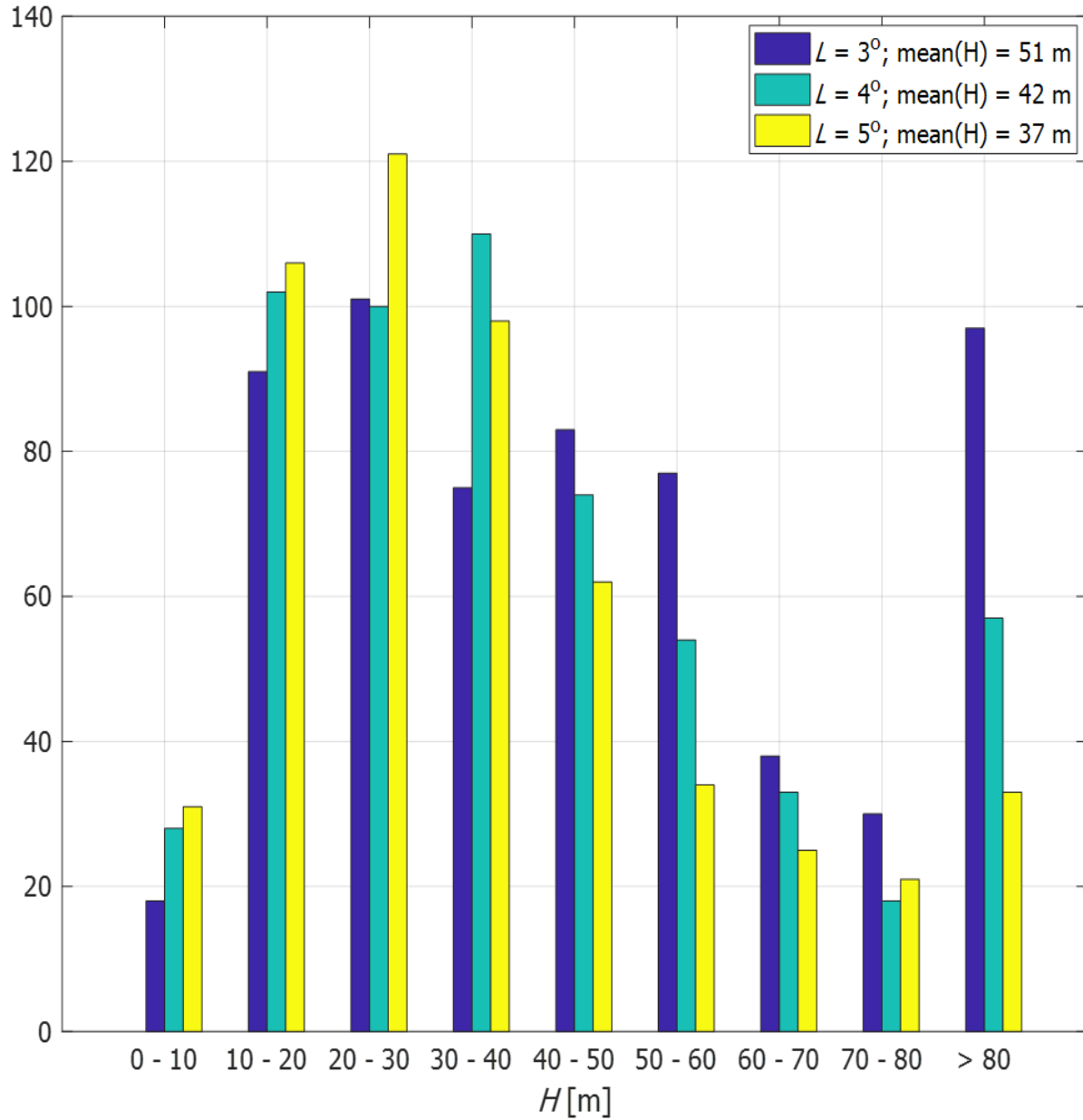
Figure 3: The histograms of H-values for the 3 values of L. For $L = 3°$ the tail of $H > 80$ m is as high as
the maximum cell of $H = 20 - 30$ m consistent with singularity of Eq. (3) at $L = y_i(0)$.

290
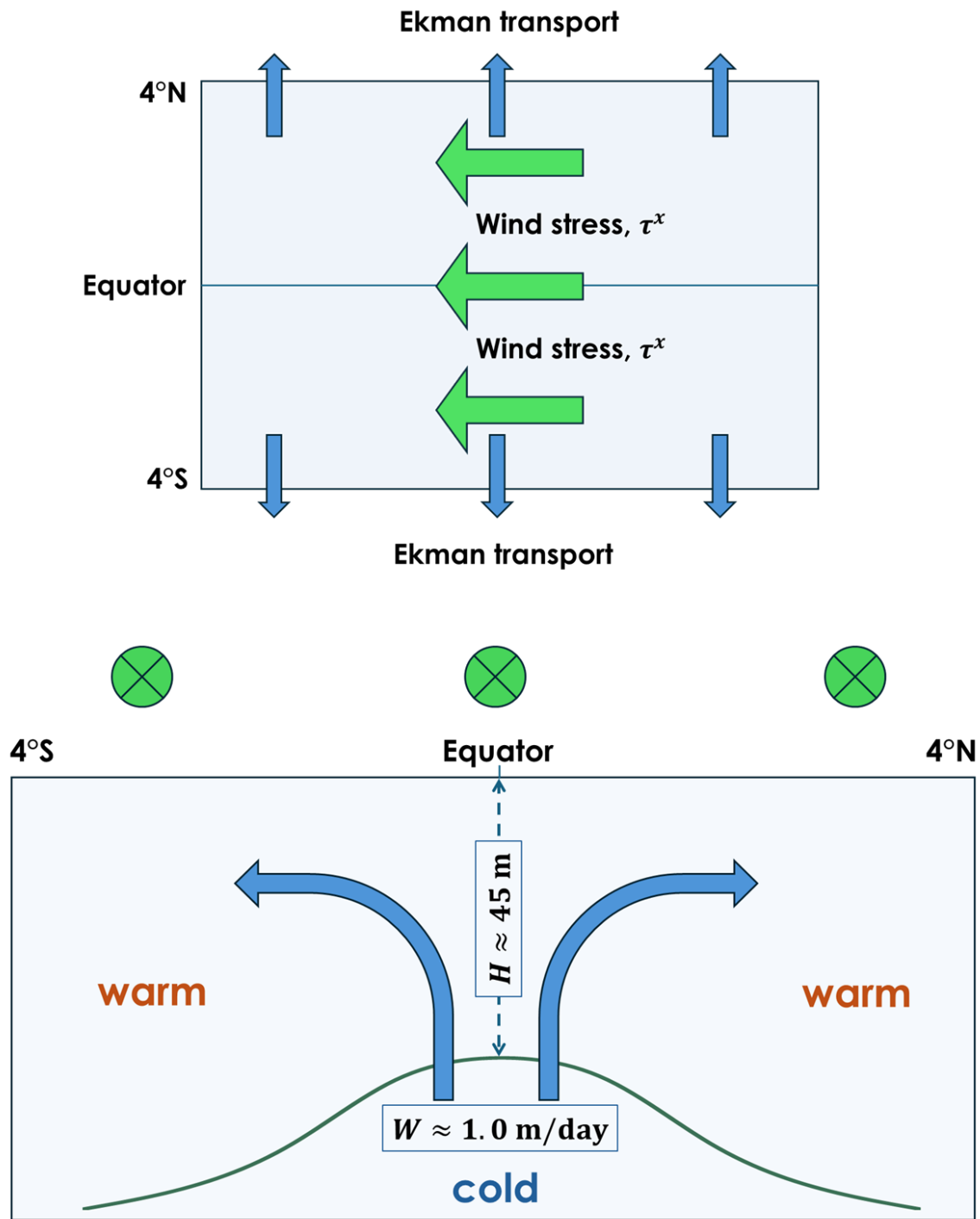
292 **Figure 4: A sketch relating the poleward directed wind-driven surface flow along the equator under**
293 **westward directed wind stress (upper panel) which is compensated by the upwelling of water from**
294 **below (lower panel). The upper panel is a planar view and the lower panel is a latitude-height cross-**
295 **section viewed from the east. The $H \approx 45$ m and $W \approx 1.0$ m day^{-1} estimates are the main results of**
296 **this study.**

References

Bubnov, V. A.: Vertical motion in the Central Equatorial Pacific. *Oceanologica Acta, Special Issue*, Gauthier-Villars. 1987.

Brady, E. C. and Bryden, H. L.: Estimating vertical velocity on the Equator. *Oceanologica Acta, Special Issue*, 1987.

Czaja, A. and Marshall, J.: The partitioning of poleward heat transport between the atmosphere and ocean. *J. Atm. Sci*., **63(5)**, 1498-1511. **https://doi.org/10.1175/JAS3695.1**, 2006.

Ekman, V. W.: On the influence of earth's rotation on ocean-currents. *Ark. Mat. Astr. Fys*., **2**, 1–52, 1905.

Goldstein, H.: *Classical Mechanics*. Addison-Wesley, Inc, 1980.

Halpern, D. and Freitag, H. D.: Vertical motion in the upper ocean of the equatorial Eastern Pacific. *Oceanologica Acta, Special Issue*, Gauthier-Villars. 1987.

Halpern, D., Knox, R. A., Luther, D. S. and Philander, S. G. H.: estimates of equatorial upwelling between 140° and 110°W during 1984. *J. Geophys. Res.:Oceans*. **94(C6)**, 8018-8020. **https://doi.org/10.1029/JC094iC06p08018**. 1989

Hansen, D. V. and Paul, C. A.: vertical motion in the Eastern equatorial Pacific inferred from drifting buoys. *Oceanologica Acta, Special Issue*, Gauthier-Villars. 1987.

Hartmann, D. L.: *Global Physical Climatology*, 2nd Ed., Elsevier Inc**. https://doi.org/10.1016/C2009-0-00030-0.** 2016.

Hastenrath, S. and Polzin, D.: Dynamics of the surface win field over the equatorial Indian Ocean. *Q. J. R. Meteorol. Soc*., **130**. 503-517. **https://doi.org/10.1256/qj.03.79**, 2004.

Johnson, G. C., McPhaden, M. J., and Firing, E.: Equatorial Pacific Ocean Horizontal Velocity, Divergence, and upwelling. *J. Phys. Oceanogr*., **31(3)**, 839-849. **https://doi.org/10.1175/1520-0485(2001)031<0839:EPOHVD>2.0.CO;2**, 2001.

Knauss, J. A.: *Introduction to Physical Oceanography*, 2nd Ed. Prentice Hall, Inc. ISBN 0-13-238155-9, 1996.

Lagerloef, G. S. E., Mitchum, G. T., Lukas, R. B. and Niiler, P. P.: Tropical Pacific near-surface currents estimated from altimeter, wind, and drifter data. *J. Geophys. Res*.: Oceans, 104(10), 23,313-23,326. **https://doi.org/10.1029/1999JC900197**, 1999.

Lukas, R. and Lindstrom, E.: The mixed layer of the western equatorial Pacific Ocean *J. Geophys. Res.: Oceans*. **96**, 3343-3357. **https://doi.org/10.1029/90JC01951**, 1991.

Lumpkin, R., Ozgokmen, T. and Centurioni, L.: Advances in the application of surface drifters. *Ann. Rev. Mar. Sci*., **9**, https://doi.org/10.1146/annurev-marine-010816-060641, 2017.

NOAA/CoastWatch: https://coastwatch.pfeg.noaa.gov/erddap/files/erdQSstress3day/erdQStaux3day/

NOAA/AOM/GDP: https://erddap.aoml.noaa.gov/gdp/erddap/tabledap/drifter_6hour_qc.html

Paldor, N. and Friedland, L.: Wind-driven transport of the spherical earth. *Phys. Fluids*, **35**, 056604. https://doi.org/10.5194/os-19-93-2023, 2023.

Paldor, N.: A Lagrangian theory of equatorial upwelling. *Phys. Fluids*, **36**, 046605. https://doi.org/10.1063/5.0202412, 2024.

335   Poulain, P.-M.: Estimates of Horizontal Divergence and Vertical Velocity in the Equatorial Pacific. *J. Phys.*
336   *Oceanogr*. **23**, 601-607. 1993.

337   Quay, P. D., Stuiver, M. and Brocker, W. S.: Upwelling rates for the equatorial Pacific Ocean derived from
338   the bomb 14C distribution. *J. Mar. Res*., **41**, 769-792. 1983.

339   RomKedar, V. Dvorkin, Y. and Paldor, N.: Chaotic Hamiltonian Dynamics of particle's motion in the
340   atmosphere. *Physica. D*, 106(3-4), 389-431. https://DOI.org/10.1016/S0167-2789(97)00015-8

341   Talley, L. D., Pickard, G. L., Emery, W. J. and Swift, J. H.: *Descriptive Physical Oceanography: An*
342   *Introduction*, 6th Ed. Academic Press. ISBN: 978-0-7506-4552-2, 2011.

343   Weingartner, T. J. and Weisberg, R. H.: On the annual cycle of equatorial upwelling in the central Atlantic
344   Ocean, *J. Phys. Oceanogr.,* **21(1)**, 68-82. https://doi.or*g/10.11*75/1520-
345   0485(1991)021<0068:OTACOE>2.0.CO;2, 1991.

346   Wyrtki, K.: An estimate of equatorial upwelling in the Pacific. *J. Phys. Oceanogr*. 11(9). 1205-1214.
347   https://doi.org/10.1175/1520-0485(1981)011<1205:AEOEUI>2.0.CO;2, 1981.

348   Zhang, L., Li, Y. and Li, J.: Impact of equatorial wind stress on Ekman transport during the mature phase of
349   the Indian Ocean Dipole. *Clim. Dyn.* **59**, 1253–1264. https://doi.org/10.1007/s00382-022-06183-7,
350   2022.